Mono- and Bichromatic Electron Dynamics: LiH, a Test Case

Angela Acocella, Garth A. Jones, and Francesco Zerbetto*

Dipartimento di Chimica "G. Ciamician", Università di Bologna, V. F. Selmi 2, 40126, Bologna, Italy

Received: January 11, 2006; In Final Form: March 3, 2006

This paper describes an electron dynamics method where the time dependence of an external oscillating electric field is the perturbing part of the Hamiltonian. Application of the electric field induces charge movement inside the molecule and electronic transitions between the molecular orbitals. The test system is the neutral LiH molecule. The method is applied to wave functions calculated using the B3LYP (hybrid) density functional, with the STO-3G and the 6-31+G basis sets. The molecule undergoes full population inversion between the HOMO and the LUMO when the electric field is in resonance with the HOMO−LUMO energy gap. The magnitude of the electric field directly affects the rate at which electronic transitions occur and the rate at which charges move between lithium and hydrogen atoms. The method is used to model both monochromatic and bichromatic multiphoton effects in LiH. Monochromatic one-, two- and three-photon transitions occur between the HOMO, LUMO and two other virtual orbitals. There is evidence of both [1+2] direct and [1+1+1] stepwise multiphoton transitions. Bichromatically, two "laser" pulses are applied at different frequencies. Electronic transitions can be fine-tuned to occur via pre-specified pathways of virtual molecular orbitals.

I. Introduction

A variety of quantum chemical approaches for the calculation of excited states are presently available. They yield energies and oscillator strengths of several states in a single calculation. Excited-state models, in analogy to the ground-state ones, can be divided into wave function-based methods and electron-density-based methods. The prototypical wave function-based method is the Hartree−Fock model, which has spawned the configuration interaction,[1] the multireference CI (MRCI),[2] multireference Møller−Plesset approaches,[3] and the multiconfigurational self-consistent field (MCSCF) methods.[4] These models are based on (additional) Slater determinants constructed from the ground state by swapping occupied with virtual orbitals.

Electron-density methods[5] rely on the electron density as the fundamental quantity. The exchange and correlation effects are compounded into the so-called exchange-correlation (xc) functional. In general, xc functionals can be divided into three different classes: local functionals, gradient-corrected functionals, and hybrid functionals.

Both approaches can be the starting point of time-dependent models where, after algebraic manipulation, one can recast the time dependency with respect to an external perturbation into an eigenvalue equation. An authoritative review of these approaches has been presented very recently.[6]

Alternatively, one can retain the time dependency of the Schrödinger equation, TDSE, and directly integrate it to generate a trajectory where the electronic occupancy changes in time as a function of the perturbation.[7,8]

In the present paper, we present a simple but efficient procedure for developing time-dependent trajectories to study the complex behavior of molecular orbitals in an intense external electric field. As with the models where oscillator strengths are of interest, the nuclear degrees of freedom are frozen and the electronic transitions and polarization effects arise only via interaction with the field.

* Corresponding author. E-mail: francesco.zerbetto@unibo.it.

The algorithm describes the quantum mechanical part of the TDSE method with a propagator. In particular, we have selected the Cayley algorithm proposed by Allen and co-workers.[8] The external perturbation is a linearly polarized electric field introduced as an oscillating wave. The molecular coefficients are updated at each time step (of the order of attoseconds) and determine how the electron density flows inside the molecule in terms of both the evolution of the orbital populations and the atomic charges.

Recently there has been a great deal of interest in developing time-dependent methods, which can model multiphoton events.[9−19] The time-dependent model developed in this paper has been applied to LiH using the 6-31+G basis set because its electronic structure (accidentally) gives rise to the possibility of competing mono-chromatic multiphoton transitions. It is shown that the time-dependent model predicts both direct and stepwise monochromatic multiphoton events, as well as bichromatic processes.

In the following sections, computational details of the method are presented, together with the analysis of an initial test application to LiH.

II. Computational Details

The intent of this work is to model (pre-ionization) electron dynamics in molecular systems when they are subject to (intense) external laser fields.

The time-dependent algorithm implemented employs the electron dynamics propagator proposed by Allen and co-workers for the tight binding Hamiltonian,[8] which reads

$$\Psi(t+\Delta t) = \left(1 + \frac{iH\Delta t}{2\hbar}\right)^{-1}\left(1 - \frac{iH\Delta t}{2\hbar}\right)\Psi(t) \qquad (1)$$

where Ψ is the electronic wave function and H is the matrix of the electronic Hamiltonian, given by the sum of the unperturbed Hamiltonian H° and the perturbed Hamiltonian H', which represents the interaction between the classical electric field and the molecular dipole moment. Because the nuclear geometry is

10.1021/jp060195i CCC: $33.50
Published on Web 03/29/2006

frozen during the electron dynamics, electronic transitions and polarization of the molecule occur strictly because of application of the electric field. The method employs as $H°$ a "fixed unperturbed Hamiltonian" where the initial orbital energies remain constant for the entire duration of the trajectory.

The initial wave function $\Psi(t=0)$, Hamiltonian $H°$, together with the optimized molecular structures are obtained with the Gaussian03 suite of programs.[20] The unperturbed Hamiltonian, $H°$ is obtained from the eigenvalues (molecular orbital energies at time $t = 0$) and the initial wave function coefficients are expressed in the atomic basis.

The perturbing part of the Hamiltonian, H' is expressed in terms of the product between the matrix of the dipole moment in the atomic basis, D, here representing the transition matrix between molecular orbitals (in the direction of the applied electric field) and a sinusoidal wave of the oscillating external feld:

$$H'(t) = -D\epsilon(t)\sin(\omega t) \tag{2}$$

where ω is the frequency of the field. In our approximation this is exactly equal to the difference between the ground-state energies of the two molecular orbital levels involved in the excitation process. The parameter ϵ is the corresponding amplitude, which may be constant (all examples considered in this paper) or change in time.

The molecular coefficients are updated at each time step because of the effect of the external field.

This approach affords a simple way to shift orbitals into- and out-of-resonance with the applied electric field (vide infra). The time evolution of the atomic orbitals coefficients under the influence of the oscillating electric field allows one to monitor the electronic occupations of the molecular orbitals:

$$\mathbf{P}_{ij}(t) = \sum_{k}^{\text{occ}} c_{ik}^{*}(t)\, c_{jk}(t) \tag{3}$$

where $\mathbf{P}_{ij}$ is the density matrix for atomic orbitals i and j, $c_{jk}(t)$ is the jth component of the k_{th} eigenvector of the initial unperturbed Hamiltonian at time t. The density matrix in the atomic orbital basis is easily transformed into the density matrix in the molecular orbital basis through a unitary transformation

$$\mathbf{P_{MO}}(t_i) = \mathbf{C_k}^{t}(0)\, \mathbf{P_{AO}}(t_i)\, \mathbf{C_k}(0) \tag{4}$$

where $\mathbf{C_k}$ contains the coefficients of the MOs expanded in the AO basis.

Importantly, the propagation is carried out starting from molecular orbitals orthonormalized by the Löwdin transformation.

Our approach, although similar to that of Schlegel and coworkers,[7] which involves direct integration of the time-dependent Schrödinger equation, produces propagation of the wave function via eq 1. One of the major approximations of the present model is the molecular Hamiltonian is fixed and the method does not include electron correlation and spin−orbit interaction terms in the electronically excited states. The primary reason for the use of this approximation is the method is intended to be applied, in the future, to large molecular systems.

III. Application of the Model

III.1. Rabi Frequency Tests for H_2^+ and LiH. To test the algorithm of eq 1, the methodology was applied to the H_2^+ molecular ion and the LiH molecule using a two-state approach, where the states are calculated from TD-B3LYP theory using the STO-3G basis set. In both cases, the external field applied was chosen to have a frequency corresponding to the energy gap between the ground and the first excited states and was oriented in the direction of the molecular axis. The transition dipole moments were used to introduce the external perturbation.

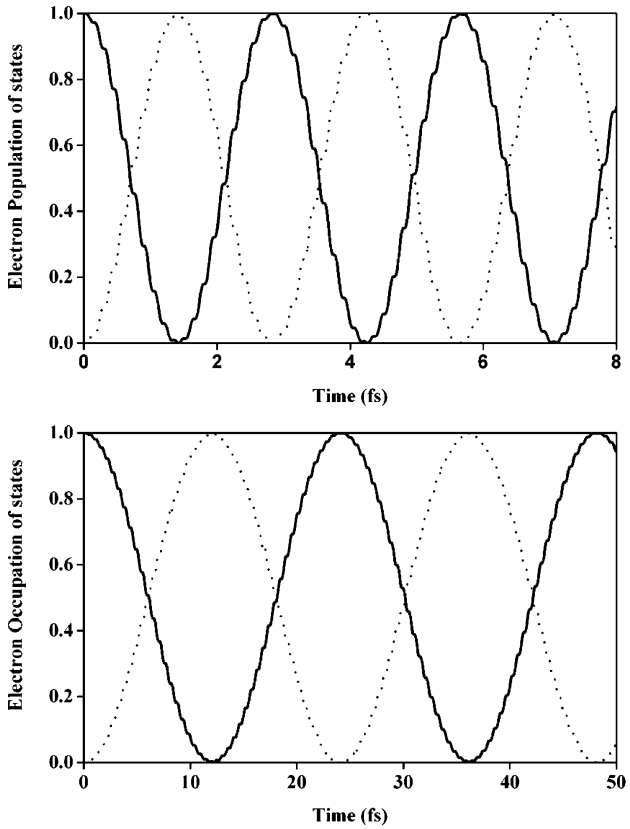

Figure 1. Top: electron population of the ground state (in solid line) and of the first excited state (in dotted line) for H_2^+ molecule. Bottom: electron population of the ground state (in solid line) and of the first excited state (in dotted line) for LiH molecule.

In a two-state system, the algorithm should be able to reproduce the Rabi frequencies. The bond length for H_2^+ was set to 1.060 and 1.145 Å for LiH. The calculated transition dipole moments, μ, are 1.0687 au and −0.3127 au, respectively. The electron dynamics simulations were run with applied electric field amplitudes, ϵ, of 0.05 atomic units for H_2^+ and 0.02 atomic units for LiH. The top half of Figure 1 shows the electronic populations of the ground and first excited states for H_2^+. The resulting Rabi frequency is 0.054 atomic units, which is in good agreement with the analytical solution of 0.056 atomic units ($(\epsilon \cdot \mu)/\hbar$). A similar study on LiH (bottom half of Figure 1), produces a Rabi frequency of 0.0063 atomic units, which compares nicely with the analytical solution of 0.0062 atomic units.

Because our major interest is in modeling processes that involve large systems and/or events that involve more than two levels (such as multiphoton processes), we will apply the electron dynamics algorithm to a standard B3LYP wave function in all other applications in this paper, as described in section II. This means that the method is more approximate than the two-state approach; however, it allows us to gain qualitative insight into complex processes that cannot be easily modeled using the two-state approach.

III.2. Population Inversion, Charge Shift and Effects of Orbital Symmetry. To investigate more complex physical properties of molecules in the presence of an intense external electric field, test calculations were run on LiH using the single

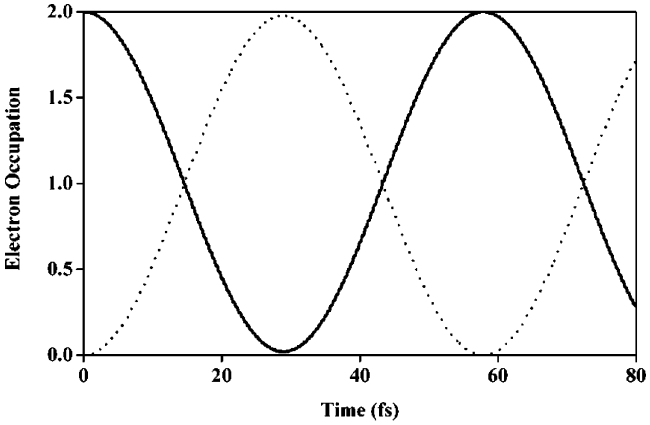

Figure 2. Occupancies of HOMO (solid line) and LUMO (dotted line) during the electron dynamics of LiH at B3LYP/STO-3G level. The electric field points along the molecular axis. The frequency of oscillation of the applied electric field corresponds to the HOMO−LUMO energy gap and the intensity is 1.028 V Å^{-1}. Note that electronic occupation of the other molecular orbitals do not change (see text for conversion to other units).

TABLE 1: MO Energies of LiH at the B3LYP/STO-3G Level of Theory

orbital	absolute energy (au)	relative energy (eV)
1 (HOMO−1)	−1.89798	−46.3349
2 (HOMO)	−0.19518	0.0
3 (LUMO)	−0.01311	4.9543
4 (LUMO+1)	0.05030	6.6798
5 (LUMO+2)	0.05030	6.6798
6 (LUMO+3)	0.4431	17.3682

Slater determinant approach, as discussed in section II. The minimal STO-3G and the larger, more accurate 6-31+G basis sets were employed. The hybrid density functional B3LYP method was used to calculate the initial wave function and the other quantities required.

The external field applied was chosen to have a frequency corresponding to the energy gap between the HOMO and the LUMO and was oriented in the direction of the molecular axis. Two-level coherent excitation was obtained for both systems, with complete population inversion.

At the B3LYP/STO-3G level, LiH has an optimized bond length of 1.145 Å. At this level of theory the system is made up of 6 MO's (two occupied and four virtual). The absolute energies (in atomic units) of all of the MO's and their relative energies with respect to the HOMO (in electronvolts) are displayed in Table 1.

Figure 2 displays the electronic occupations of the HOMO and the LUMO, as a function of time (in femtoseconds). The electric field is applied in the direction of the molecular axis (the *z*-direction) with a frequency corresponding to the energy gap between the HOMO and the LUMO (4.9 eV), and an intensity of 1.028 V Å^{-1} (corresponding to 0.02 atomic units, or in units of power per surface area 3.50×10^{13} W cm^{-2}). Unless otherwise stated, this field strength is used and all intensities considered fall below that required to cause ionization.[21] The model does not currently account for ionization. HOMO and LUMO undergo complete population inversion after ∼30 fs.

Figure 3 is a magnification of the first eight femtoseconds of Figure 2. The size of the perturbation is also shown in the right-hand *y*-axis of the plot.

The oscillations in occupancy at higher frequency correspond to the characteristic frequency of the perturbation. The amplitude

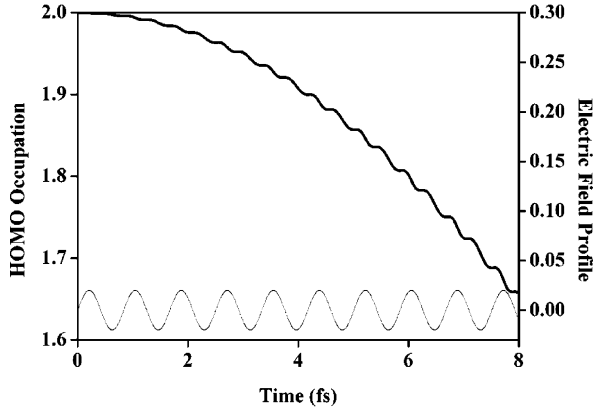

Figure 3. Blow up of Figure 2. HOMO occupancy (solid line) during the electron dynamics of LiH at B3LYP/STO-3G level and magnitude of the oscillating electric field perturbation (dotted line, right ordinate, displayed in au). The amplitude of the electric field is 1.028 V Å^{-1} (see text for conversion to other units).

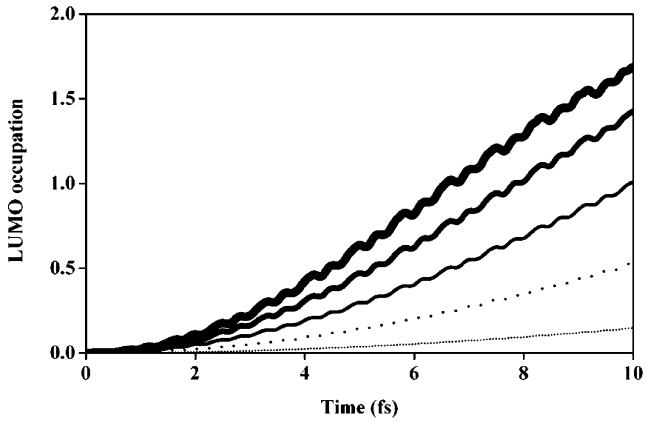

Figure 4. Rate of electronic population of the LUMO for five different electric field intensities. The intensities are 0.514, 1.028, 1.542, 2.056, and 2.570 V Å^{-1}. The rate of occupation of the LUMO is proportional to the strength of the field.

of the perturbation directly affects the rate at which the electronic occupancies of the MO's change. Increasing the amplitude of the perturbation, while maintaining the same frequency of oscillation, results in an increase in the rate at which electrons move between the orbitals. This is confirmed in a series of five calculations carried out with a range of intensities from 0.514 to 2.570 V Å^{-1} and intermediate values of 1.028, 1.542, and 2.056 V Å^{-1}.

Figure 4 shows that when the molecule is subject to the most intense electric field (2.570 V Å^{-1}), the electrons move from the HOMO to the LUMO extremely rapidly, whereas a reduction of the amplitude of the field results in the rate of electron movement proportionally lower. Full population inversion occurs after 12.6 and 56.8 fs, respectively, for the strongest (2.570 V Å^{-1}) and the weakest (0.514 V Å^{-1}) electric fields.

The six MO's of LiH calculated at the B3LYP/STO-3G level are displayed in Figure 5. The HOMO−1, HOMO, LUMO and LUMO+3 are σ-orbitals and are symmetric in the *xz*- and the *yz*-planes, whereas the degenerate pair of π-orbitals (the LUMO+1 and LUMO+2) are antisymmetric with respect to the *yz*- and *xz*-planes. For transitions to occur from the HOMO to the π-orbitals, the electric field must transform as the *x*-direction to reach the LUMO+1, and as the *y*-direction to reach the LUMO+2.

To verify that the model obeys the symmetry requirements, the molecule was subjected to an electric field with a frequency

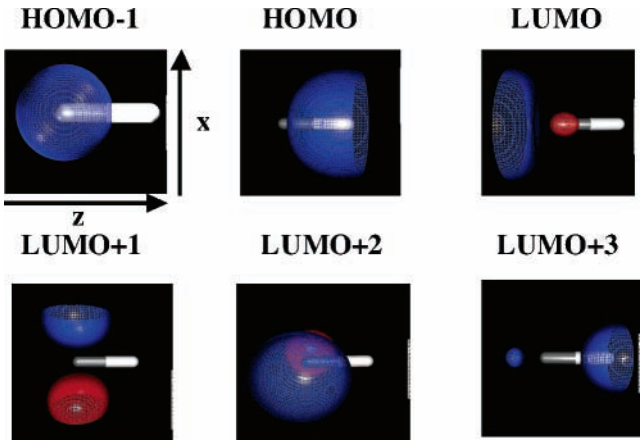

Figure 5. Molecular orbitals of LiH at the B3LYP/STO-3G level (Li atom is on the left). Note that the LUMO+1 and LUMO+2 are degenerate π-orbitals. The LUMO+1 is antisymmetric with respect to the *yz*-plane, and the LUMO+2 is antisymmetric with respect to the *xz*-plane.

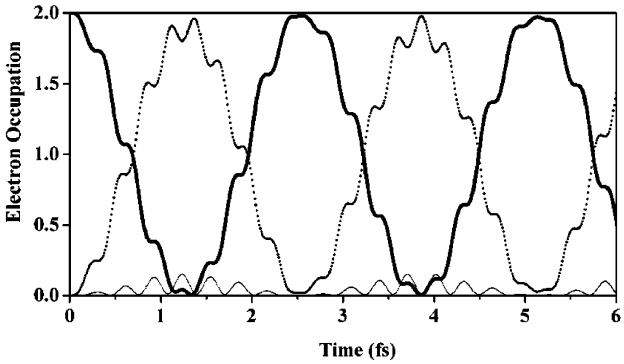

Figure 6. Occupancies of HOMO (solid line), LUMO (thin solid line), and one of the degenerate π_x-orbital (dotted line), when the applied electric field is in the *x*-direction. The frequency corresponds to the energy gap between the HOMO and the degenerate pair of π-orbitals (6.68 eV) and the intensity is $\epsilon = 1.028$ V Å^{-1}. Under these conditions the electrons primarily enter the π_x-orbital. Only a small fraction enters the LUMO, which never exceeds an occupancy of 0.2.

corresponding to the energy gap between the HOMO and the degenerate pair of virtual π-orbitals. The field was applied in both the *x*- and *y*-directions (with an intensity of 1.028 V Å^{-1}). Correctly, electrons from the HOMO move rapidly into the π-orbital whose symmetry is "broken" by the applied electric field. Furthermore, only a very small fraction of electrons enter the LUMO because this transition is out-of-resonance with the applied electric field and the effect is not a proper transition but a polarization of the wave function. Figure 6 shows the occupation of the relevant orbitals in time, when the external electric field is applied in the *x*-direction. The electron moves rapidly between the HOMO and the π_x-orbital and there is almost complete population inversion within 1.4 fs.

Figure 7 gives the time dependence of the number of electrons on the lithium atom (this is obtained by summing the electron occupation of the atomic orbitals localized on the Li atom) when the applied electric field has a frequency corresponding to the HOMO−LUMO energy gap. It shows the variation of electron localization in time using three different electric field intensities, 0.514, 1.542, and 2.570 V Å^{-1}. One can see that the number of electrons on lithium oscillates with two frequencies (as is the case of the electron occupation). The faster frequency is directly related to the frequency of perturbation, and the slower frequency is essentially the rate of electron transfer between

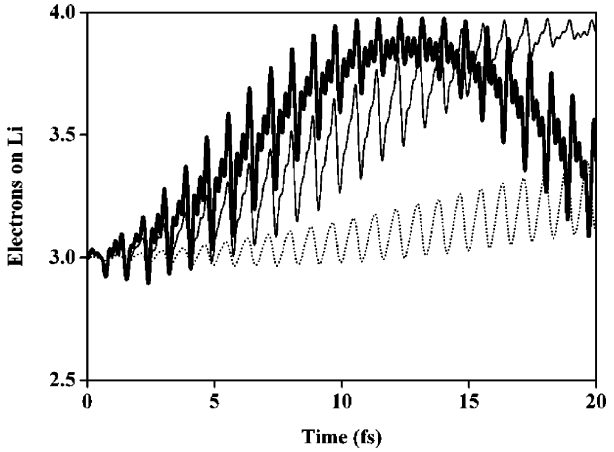

Figure 7. Time dependence of the number of electrons localized on the lithium atom. Electric field intensities: 0.514 (thick solid line), 1.542 (medium solid line), and 2.570 (light dotted line) V Å^{-1}.

the H and Li atom. With the STO-3G basis set, the number of electrons localized on Li is rarely less than three, with the simulations indicating that the electron is transferred from hydrogen to lithium. In the most intense field (2.570 V Å^{-1}) 0.96 of the electron is fully relocated to the Li after 10.6 fs, and for the weakest field (0.514 V Å $^{-1}$) 0.96 of the electron is relocated after 50.6 fs. Note that these numbers are very similar to the rates of electronic transition to the LUMO under the same fields (vide supra).

A final test was made to ensure that the model did not produce a "false positive" result. LiH was subjected to an applied electric field with a frequency that was *not-in-resonance* with any of the energy gaps corresponding to a transition between any molecular orbitals. In this case no transition should be possible, and the HOMO and HOMO−1 should maintain close to full occupancy. A simulation was run, with the frequency of the external electric field (along the direction of the molecular axis) corresponding to $\sqrt{2}$ divided by the HOMO−LUMO energy gap ($\epsilon = 1.028$ V Å^{-1}). The $\sqrt{2}$ factor was chosen for a purely pedantic reason because this is an irrational number and therefore should not correspond to any kind of multiphoton event for the HOMO−LUMO transition (even with an infinite amount of photons). The resulting frequency is not in resonance with any of the other transitions. The time-dependent model correctly predicts that no electronic transitions occur and the HOMO retains constant occupancy of two electrons.

III.3. Monochromatic Multiphoton Processes. The time-dependent model was then applied using the larger and more accurate 6-31+G basis set. At this level of theory there are two doubly occupied and 13 virtual orbitals. As expected, the model gives results qualitatively similar to those of the STO-3G level. However, the 6-31+G basis set produces a richer electronic structure and two- and three-photon events are also observed after a few femtoseconds.

Table 2 gives the molecular orbital energies (in atomic units), the energies relative to the HOMO (in electronvolts) and the ratio of the energy gaps between the higher virtual orbitals and the HOMO, and the HOMO−LUMO energy gap. The ratios displayed in column four of Table 2 for MO's 10 and 14 are integers. This means that electrons may be promoted to these orbitals via monochromatic multiphoton mechanisms. LiH may therefore absorb more than one photon at the HOMO−LUMO transition frequency, thereby allowing electronic transitions to the higher energy virtual orbitals. Three rows of the Table 2 are in bold. The transition to the first orbital, number 3,

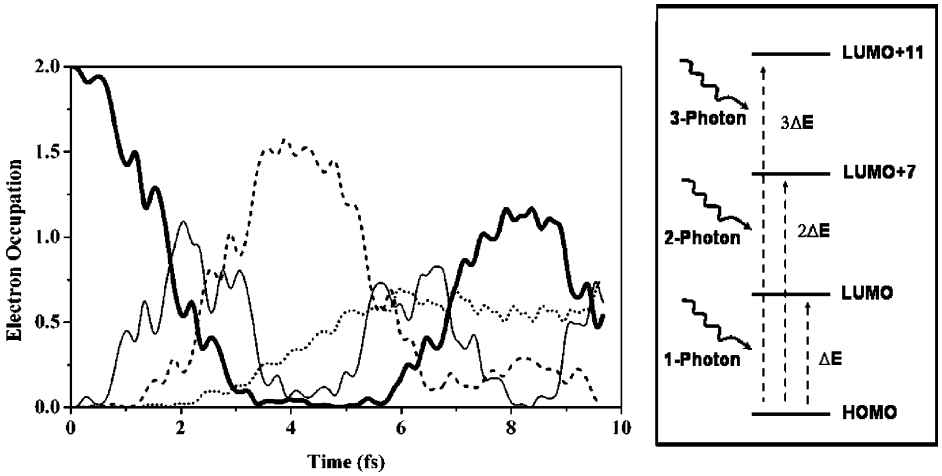

Figure 8. Time evolution of the HOMO (solid line), LUMO (light solid line), LUMO+7 (dashed line) and LUMO+11 (dotted line). Occupation of the LUMO+7 and LUMO+11 occurs after longer times via multiphoton processes. The frequency of the applied electric field is in resonance with the HOMO−LUMO energy gap, and its intensity is 1.028 V Å^{-1}. A cartoon representation of the (monochromatic) multiphoton processes given on the right.

TABLE 2: Absolute Energies, Energies Relative to HOMO, and Ratios with Respect to the HOMO−LUMO Energy Gap for the MO's of LiH at the B3LYP/6-31+G Level

orbital	absolute energy (au)	relative energy (eV)	fractional energy
1	−2.00935	−49.33	N/A
2 (HOMO)	−0.19651	0.00	N/A
3 (LUMO)	**−0.04800**	**4.04**	**1.00**
4	−0.00888	5.01	1.24
5	−0.00888	5.01	1.24
6	0.00658	5.53	1.26
7	0.01381	5.72	1.42
8	0.02404	6.00	1.49
9	0.02404	6.00	1.49
10 (LUMO+7)	**0.10022**	**8.07**	**2.00**
11	0.14606	9.32	2.31
12	0.14606	9.32	2.31
13 (LUMO+10)	0.16943	9.96	2.47
14 (LUMO+11)	**0.24803**	**12.10**	**3.00**
15	1.05222	33.97	8.41

corresponds to a normal one-photon transition, whereas to the second (orbital 10) and the third (orbital 14) correspond to two- and three-photon transitions. Figure 8 displays the multiphoton process diagrammatically. As in the STO-3G case, the applied electric field was directed along the molecular axis with a frequency corresponding to the HOMO−LUMO energy gap (4.04 eV or 0.149 au) and an amplitude of 1.028 V Å^{-1}.

Notice that HOMO, LUMO, LUMO+7, and LUMO+11 belong to the Σ irreducible representation and one-, two- and three-photon transitions are all equally symmetry-allowed.

Figure 8 shows the time evolution of the occupancies of the HOMO and the three virtual orbitals to which electronic transitions may occur when the electric field has a frequency in resonance with the HOMO−LUMO energy gap. Electrons rapidly begin to leave the HOMO and within ∼3.4 fs the HOMO has close to zero occupancy. The HOMO remains empty for over 2 fs, and during this time the electrons move solely between the virtual orbitals. One can see that the unoccupied orbitals become successively occupied according to their increasing energy. This may indicate (see below) that the multiphoton events primarily occur via a stepwise mechanism. The multiphotonic process can be interpreted as follows: the occupancy of the LUMO increases rapidly within the second femtosecond and has electron occupancy equal to one by this time. Then the LUMO+7 begins to take on electron occupancy after a further femtosecond. At ∼3.0 fs, the time dependencies of the LUMO and the LUMO+7 occupancies become near mirror images of each other. The curves are strongly coupled. This clearly indicates that the electron is moving directly from the LUMO to the LUMO+7. That is the two-photon event occurs via a [1+1] stepwise mechanism; the first one-photon absorption induces the HOMO-to-LUMO transition, and the second subsequent absorption produces the LUMO-to-LUMO+7 transition. The third virtual orbital that takes on sizable electron occupation is the LUMO+11. From Figure 8, one can also see that electron occupation moves into this orbital at a much slower rate relative to the other orbitals. This is probably because the LUMO+7 must be significantly occupied before the electron density can move from there to the LUMO+11 via a [1+1+1] three-photon event.

To determine whether the multiphoton events occur strictly via a [1+1+1] stepwise mechanism, or whether a direct mechanism is also involved, simulations were run on LiH with the intermediate virtual orbitals involved in multiphoton transitions taken out-of-resonance with the applied electric field. This is achieved by increasing the energy of the molecular orbital, setting it 20 atomic units higher than the HOMO. In practice, the Hamiltonian matrix is calculated through a unitary transformation of the diagonal matrix of the energies with the orbitals matrix, with one of the eigenvalues increased. See the schematic diagram on the right side of Figure 9 where the LUMO is taken out of resonance of the applied electric field.

Figure 9 shows the electron occupancies of the HOMO, LUMO, LUMO+7 and LUMO+11 for a trajectory where the LUMO is taken out-of-resonance with the field. Figure 9 shows that the HOMO loses less than 0.08 electron occupation and, no electrons enter the LUMO, LUMO+7, or LUMO+11. This indicates that in the case of the trajectory described for Figure 8 (where the LUMO is kept in resonance), only electrons originating from the LUMO move into the LUMO+7 and LUMO+11.

A similar simulation was also run where the LUMO+7 was taken out-of-resonance with the applied electric field, while keeping the LUMO in resonance. This is shown schematically in Figure 10, which also shows the time evolution of the HOMO, LUMO, LUMO+7, and the LUMO+11. Initially, there is a direct correlation between the increasing occupation of the LUMO and decreasing occupation of the HOMO. These are the only two orbitals involved in the process at this point of

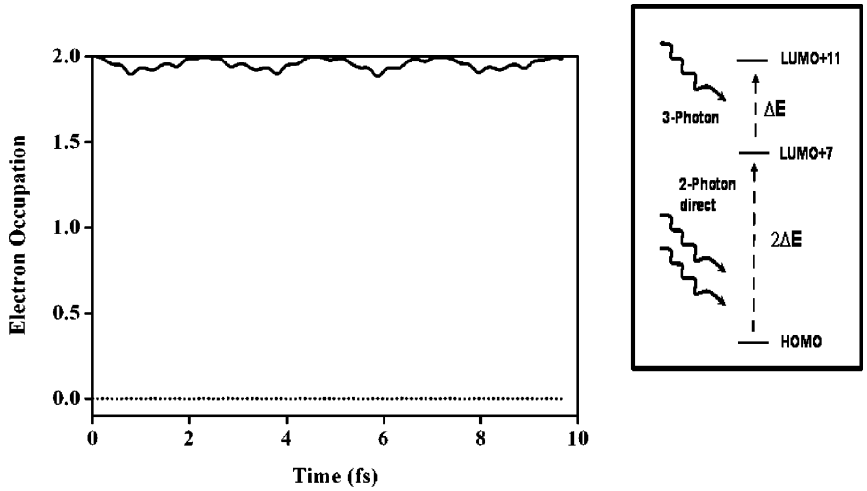

Figure 9. Electronic occupancies of the HOMO (solid line) and the LUMO, LUMO+7 and LUMO+11 (dotted line) when the HOMO−LUMO energy gap is not in resonance with the applied electric field. The intensity of the applied electric field is 1.028 V Å^{-1}. A cartoon representation of the processes, which may give rise to electronic excitation to the LUMO+7 and the LUMO+11 when the LUMO is taken out of resonance, is given on the right. Excitation to the LUMO+7 can only occur via direct two-photon absorption.

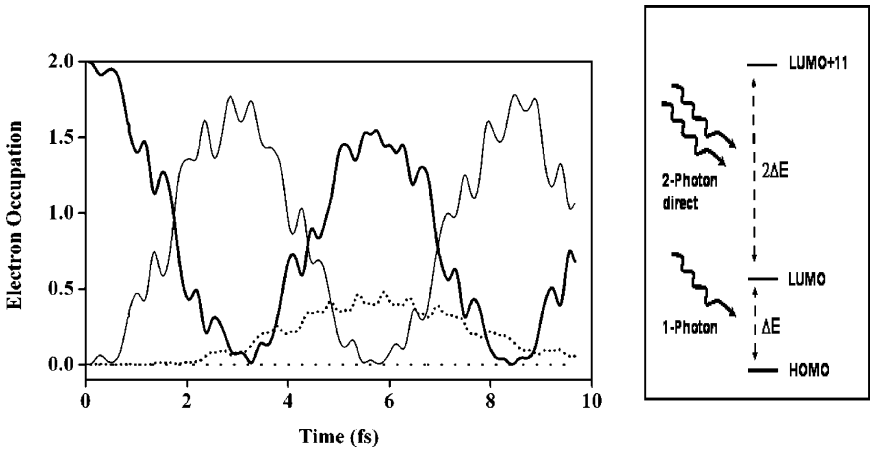

Figure 10. Electronic occupancies of the HOMO (thick solid line), LUMO (thin solid line), LUMO+7 (spaced dotted line) and LUMO+11 (dotted line) when the LUMO+7 is taken out of resonance with the applied electric field. The intensity of the electric field is 1.028 V Å^{-1}. A cartoon representation of multiphoton transitions when the LUMO+7 is taken out-of-resonance is given on the right. Excitation to the LUMO may occur via a one-photon transition, whereas excitation to the LUMO+11 must occur via a direct two-photon transition from the LUMO.

the trajectory. The electron occupation of the HOMO decreases until it becomes zero at approximately 3.2 fs. After the electron occupation of the LUMO becomes significantly large, the LUMO+11 begins to gain electron occupancy. The LUMO+7 is out-of-resonance with the applied electric field and does not gain any electron occupation during any point of the trajectory. Occupation of the LUMO+11 occurs via a direct [1+2] two-photon transition from the LUMO. By considering the time dependencies of the occupation of the LUMO+11 from the two different trajectories of Figures 8 and 10, it is possible to determine approximately when the two different multiphoton processes are occurring.

For the case of the trajectory of Figure 8, all three virtual MO's (LUMO, LUMO+7 and LUMO+11) are in resonance with the field for the respective multiphoton processes. Consequently, the occupation of the LUMO+11 in Figure 8 results from all one-, two- and three-photon transitions from the LUMO+7, LUMO and HOMO. In the case of the trajectory of Figure 10, the LUMO+7 has been taken out-of-resonance with the field and hence electron occupation of the LUMO+11 can only occur via direct two- and three-photon events from the LUMO and HOMO. However, from the trajectory of Figure 9 it is known that electronic transitions do not occur directly from the HOMO to the LUMO+11. Therefore, subtracting the electron occupancy of the LUMO+11 of Figure 10 with that of Figure 8, gives a good indication of the fraction of electronic transitions to the LUMO+11, which originate solely from the LUMO+7. This should provide an estimate of the times in the trajectory when transitions to the LUMO+11 are occurring via a [1+1+1] three-photon stepwise mechanism (Figure 8) and when they are occurring via a [1+2] direct multiphoton excitation (Figure 10).

The top part of Figure 11 displays the electronic occupation of the LUMO+11 for two different trajectories. The solid line represents the standard trajectory, where all electronic transitions are allowed between the HOMO, LUMO, LUMO+7, and LUMO+11. The dotted line represents the electronic occupation of the LUMO+11 for the trajectory where the LUMO+7 is taken out of resonance. One can see from Figure 11 that no transitions to the LUMO+11 occur during the first two femtosecond of the trajectory. Until the fourth femtosecond, both occupancies increase at similar rates, indicating that the majority of transitions to the LUMO+11 occur from the LUMO via a direct [1+2] transition. Clearly, these are the only transitions to the LUMO+11 that can occur at this point in the trajectory because the LUMO+7 is not significantly occupied. During the fourth femtosecond of the trajectory, the "solid" data set begins to increase more rapidly than the "dotted" data set, and after 6

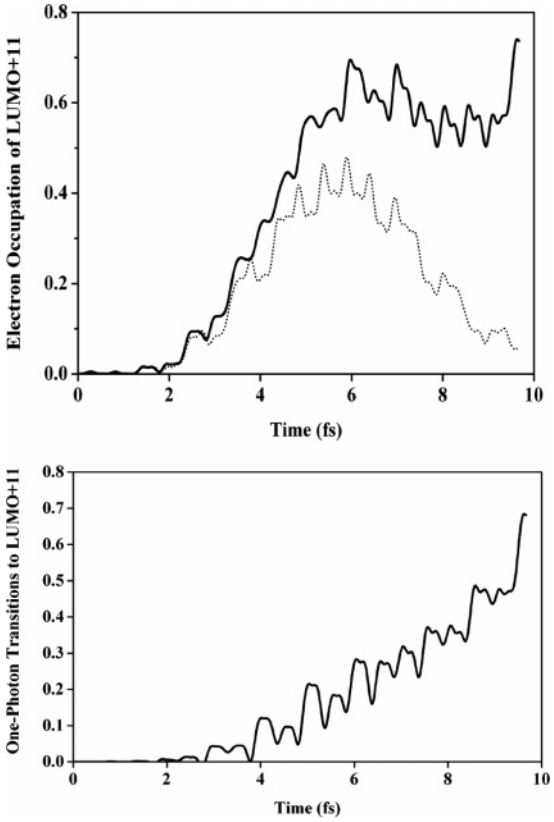

Figure 11. Top: electronic occupancy of the LUMO+11. For one trajectory, the LUMO, LUMO+7, and LUMO+11 are all in resonance (solid line), in the other, the LUMO+7 is out-of-resonance (dotted line). The field intensity is 1.028 V Å^{-1}. Bottom: amount of one-photon transitions from the LUMO+7 to the LUMO+11, calculated by subtracting the solid line from the dotted line in the top part of the figure.

fs the solid data set reaches a plateau, whereas the dotted data set begins to decrease until it becomes smaller than 0.2 at 10 fs. This corresponds to the point in the trajectory where electron occupation of the LUMO+7 dominates and the LUMO becomes empty. The now significantly occupied LUMO+7 is able to donate electron density to the LUMO+11. That is, between the 6 and 10 fs point all transitions occur via the [1+1+1] stepwise mechanism, with electron density moving from the HOMO to LUMO to LUMO+7 and finally the LUMO+11.

When the field is increased, the trend of the electron occupation of the LUMO+11 (not shown) for the trajectory in which the LUMO+7 is in resonance with the field is almost identical to the trajectory where the LUMO+7 is out-of-resonance with the field. This indicates that by increasing the amplitude of the applied electric field almost all of the transitions to the LUMO+11 occur via a [1+2] direct multiphoton transition.

In summary, the data in Figure 9 show the electron occupation of the four "active orbitals" for a trajectory where the LUMO is taken out-of-resonance with the field. In this case there is never any significant electron occupation in the LUMO or any of the other MO's. This indicates that transitions from the HOMO to the LUMO are essential to induce higher order multiphoton transitions. For trajectories where HOMO-to-LUMO transitions are allowed, further transitions to higher orbitals may occur via both direct and stepwise multiphoton events. When the intensity of the applied electric field is increased, nearly all of the multiphoton electronic transitions appear to occur via the [1+2] direct mechanism.

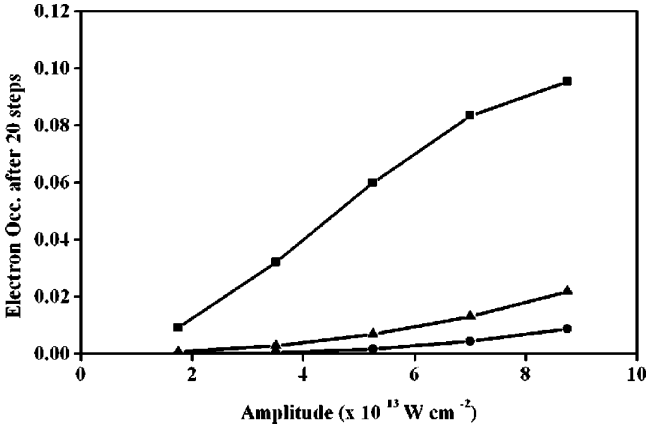

Figure 12. Electronic occupancies of the LUMO (squares), LUMO+7 (circles), and LUMO+11 (triangles) after 0.2 fs with fields of 0.514, 1.028, 1.542, 2.056, and 2.570 V Å^{-1}. All three orbitals are in resonance for multiphoton events.

TABLE 3: Quadratic Fits to the Data Points Displayed in Figure 12[a]

orbital	quadratic fit	correlation| coefficient
LUMO	$E = -0.02418 + 0.01919\epsilon - 0.00061\epsilon^2$	0.997
LUMO+7	$E = 0.00147 - 0.00114\epsilon + 0.00023\epsilon^2$	0.999
LUMO+11	$E = 0.00099 - 0.00076\epsilon + 0.00036\epsilon^2$	0.999

[a] E is the electron occupation of the orbital after 0.2 fs, ϵ is the amplitude of the electric field.

The final study conducted on monochromatic multiphoton processes in LiH involves a series of trajectories in different electric field intensities. In all cases the electric field is in resonance with the energy gaps between the HOMO and the LUMO, LUMO+7, and LUMO+11. The electric field amplitudes that were applied are 0.514, 1.028, 1.542, 2.056, and 2.570 V Å^{-1}. The objective was to determine how changes in the amplitude of the electric field affect the rate of occupation of the active virtual orbitals involved in the multiphoton processes. The electron occupation displayed corresponds to the 0.2 fs point of the trajectories (20 time steps after the electric field is switched on). The 0.2 fs mark of the trajectories was chosen because one would expect that all transitions to the virtual orbitals should occur directly from the HOMO (and not from a virtual orbital that has become recently occupied, as is the case of indirect transitions). Notice that 0.2 fs may seem a very short time but is achievable with the recently developing area of attosecond spectroscopy.[22] Figure 12 displays the electronic occupations of the LUMO, LUMO+7, and LUMO+11 as a function of the amplitude of the applied electric field for trajectories where the LUMO, LUMO+7, and LUMO+11 are in resonance with the field. The electron occupations are 9.19 $\times$ 10^{-3}, 6.33 $\times$ 10^{-5}, and 6.90 $\times$ 10^{-4} electrons for the LUMO, LUMO+7 and LUMO+11, in the case of the weakest electric field (0.514 V Å^{-1}), and 0.095, 0.009, and 0.022 electrons for the most intense electric field (2.570 V Å^{-1}). One can see that the increase in the electron occupation of the LUMO occurs approximately linearly. In the case of the occupation of the LUMO+7 and the LUMO+11, the increase in occupation as a function of the electric field is clearly nonlinear, as one would expect for multiphoton process. Quadratic functions were fitted to the three curves in Figure 12 with the results displayed in Table 3.

The quadratic fits displayed in Table 3 confirm that multiphoton events occur in the case of the LUMO+7 and LUMO+11. For the LUMO, the electronic occupation increases

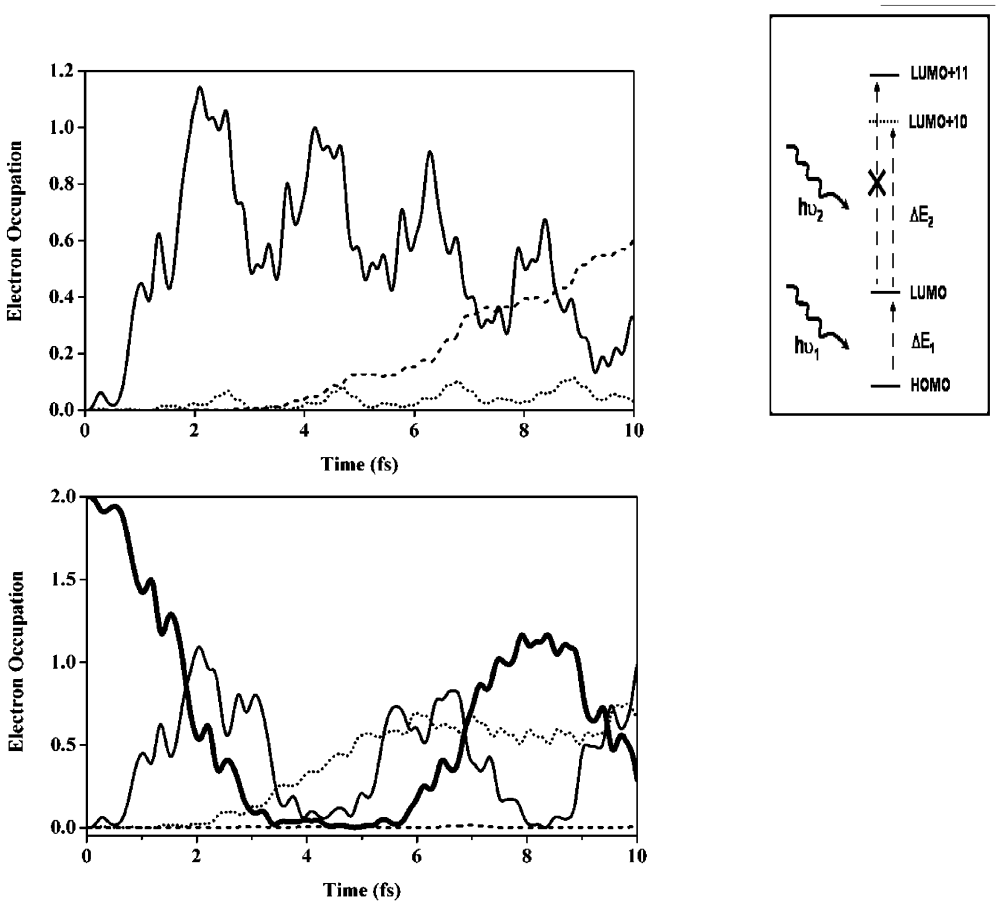

Figure 13. Top left: electron occupancies of the LUMO (solid line), LUMO+10 (dashed line), and LUMO+11 (dotted line) when a 2 fs "electric field pulse" is applied with a frequency in resonance with the HOMO−LUMO energy gap, followed by an "electric field pulse" with frequency in resonance with the LUMO−LUMO+10 energy gap. Three-photon excitation to the LUMO+11 does not occur and instead the LUMO+10 becomes occupied, e = 1.028 V Å^{-1}. Bottom left: Electron occupancies for the HOMO (thick solid line), LUMO (thin solid line), LUMO+10 (dashed line) and LUMO+11 (dotted line) when a continuous electric field is applied in resonance with the HOMO−LUMO energy gap. Excitation to the LUMO+11 occurs via a three-photon process. The intensity of the electric field is 1.028 V Å^{-1}. Left: cartoon representation of a two-photon, bichromatic process is shown on the right. The first "laser pulse" with frequency $h\nu_1$ excites electron occupation from the HOMO to the LUMO. The second longer pulse, at with frequency $h\nu_2$ pumps electrons into the LUMO+10.

linearly with the electric field amplitude. The quadratic two-photon contribution becomes important for the transitions to the LUMO+7 and to the LUMO+11. The above study indicates that by increasing the magnitude of the electric field, the number of multiphoton transitions increases. It can be clearly seen that excitation to the virtual orbitals occurs more rapidly when more intense electric fields are applied. Excitation to the LUMO+11 occurs more rapidly than to the LUMO+7 as the magnitude of the electric field is increased.

III.4. Bichromatic Two-Photon Excitation. The time-dependent model can also be used to simulate excitations with two short pulses of different frequencies. The pulses described here are sudden pulses in the sense that, when switched "on", they immediately have full intensity and, when "switched off", the perturbation becomes zero instantaneously. Both pulses are directed along the molecular axis. Here we seek to initially populate the LUMO using a 2 fs "laser" pulse, with a frequency corresponding to the energy gap between the HOMO and LUMO. After 2 fs, another longer pulse is applied for 8 fs. The second pulse is applied immediately after the first is switched off, allowing no electronic relaxation from the LUMO. The frequency of this pulse is in resonance with the energy gap between the LUMO and the LUMO+10. The aim of this trajectory is to see whether it is possible to stop the monochromatic three-photon excitation (vide supra) from occurring, leaving the LUMO+11 vacant, while forcing an electronic transition from the (now occupied) LUMO to the LUMO+10. This is described diagrammatically in Figure 13.

Figure 13 shows time dependencies of the electronic occupancies of the HOMO, LUMO+10, and LUMO+11 for two different simulations. The bottom left of Figure 13 displays the occupancies when a continuous electric field is applied with a monochromatic frequency in resonance with the HOMO−LUMO energy gap (vide supra), and the top left of Figure 13 shows electron occupations for the case described in the cartoon of Figure 13. The first pulse, with a frequency corresponding to the energy gap between the HOMO and LUMO (4.04 eV) is applied for 2 fs, whereas the second pulse, which has a frequency corresponding to energy gap between the LUMO and LUMO+10 (5.92 eV), is applied for 8 fs.

As seen earlier, application of a continuous oscillating electric field with the HOMO−LUMO characteristic frequency gives rise to occupation of the LUMO+11 via a three-photon transition. Electron occupation of the LUMO, LUMO+10, and LUMO+11 for the "two-pulse" trajectory is shown in Figure 13. Electron occupation into the LUMO+10 begins to take place at approximately the 4 fs point of the trajectory, approximately 2 fs after the second pulse is applied. Occupation of the LUMO+10 continues to increase during the period that the second pulse is applied. One can see that the occupancy of the LUMO also decreases during this period, indicating that the electron occupation of the LUMO+10 comes primarily from

the LUMO. After approximately 6.5 fs, the occupancy of the LUMO decreases, whereas that of the LUMO+10 remains constant. It can be seen that almost all of the occupancy from the LUMO moves into the HOMO (thick solid data set). Also note that the electron occupancy of the LUMO+11 remains very small during the entire trajectory because the three-photon event cannot occur once the second frequency pulse kicks in.

IV. Concluding Remarks

This paper describes the implementation and first results of an electron dynamics method, where the time dependence is built into the perturbed part of the Hamiltonian operator via an external oscillating electric field. Application of the electric field induces charge movement inside the molecule and electronic transitions between the molecular orbitals.

The test system was the neutral LiH molecule. The method was applied to wave functions calculated using the B3LYP (hybrid) density functional, using both the STO-3G and the 6-31+G basis sets. Using the STO-3G wave function, it was shown that the molecule undergoes full population inversion between the HOMO and the LUMO when the electric field is in resonance with the HOMO−LUMO energy gap. It was also shown that the magnitude of the electric field applied directly affects the rate at which electronic transitions occur and the rate at which charge moves between the lithium and hydrogen atoms. The model is also shown to obey the constraints of electronic transitions between molecular orbitals of opposing symmetry by application of the electric field in different directions.

Using the 6-31+G basis set, the model was shown to detect both monochromatic and bichromatic multiphoton effects. In the case of monochromatic multiphoton effects, one-, two- and three-photon transitions occurred between the HOMO, LUMO, LUMO+7, and LUMO+11, which are all evenly separated in energy using this basis set. Both [1+2] direct and [1+1+1] stepwise multiphoton transitions are seen to occur. In the case of bichromatic multiphoton events, two "laser" pulses are applied at different frequencies. Here the model is able to force electronic transitions to occur via pre-specified pathways by "kicking" the electron from one virtual molecular orbital to another.

Acknowledgment. Partial support from EU programs is gratefully acknowledged.

References and Notes

(1) Carsky, P. In *Encyclopedia of Computational Chemistry*; Schleyer, P. v. R., Clark, N. L., Gasteiger, J., H. F. S., III, Schreiner, P. R., Eds.; Wiley: Chichester, U.K., 1998; p 485. Kutzelnigg, W. *J. Mol. Struct. (THEOCHEM)* **1988**, *181*, 33.

(2) Buenker, R. J.; Peyerimhoff, S. D.; Butscher, W. *Mol. Phys.* **1978**, *35*, 771. Buenker, R. J.; Peyerimhoff, S. D.; Bruna, P. J. In *Computational Theoretical Organic Chemistry*; Csizmadia, I. G., Daudel, R., Eds.; Reidel: Dordrecht, The Netherlands, 1981; p 91.

(3) McDonall, J. J.; Peasley, K.; Robb, M. A. *Chem. Phys. Lett.* **1988**, *148*, 183. Andersson, K.; Malmqvist, P.-Å.; Roos, B. O. *J. Chem. Phys.* **1992**, *96*, 1218.

(4) McWeeny, R.; Sutcliffe, B. T. *Methods of Molecular Quantum Mechanics*; Academic Press: London, 1969. Roos, B. O. *Adv. Chem. Phys.* **1987**, *69*, 399. Andersson, K.; Roos, B. O. In *Modern Electronic Structure Theory*; Yarkony, D. R., Ed.; World Scientific: New York, 1995; Vol. 1, p 55.

(5) Parr, R. G.; Yang, W. *Density-Functional Theory of Atoms and Molecules*; Oxford Science Publication: New York, 1989. Dreizler, R. M.; Gross, E. K. U. *Density Functional Theory*; Springer-Verlag: Heidelberg, Germany, 1995. Baerends, E. J.; Gritsenko, O. V. *J. Phys. Chem. A* **1997**, *101*, 5383.

(6) Dreuw, A.; Head-Gordon, M.; *Chem. Rev.* **2005**, *105*, 4009.

(7) Li, X.; Smith, S. M.; Markevitch, A. N.; Romanov, D. A.; Levis, R. J.; Schlegel, H. B. *Phys. Chem., Chem. Phys.* **2005**, *7*, 233. Smith, S. M.; Li, X.; Markevitch, A. N.; Romanov, D. A.; Levis, R. J.; Schlegel, H. B. *J. Phys. Chem. A* **2005**, **109**, 5176.

(8) Allen, R. E. *Phys. Rev. B* **1994**, *50*, 18629. Graves, J. S.; Allen, R. E. *Phys. Rev. B* **1998**, *58*, 13627. Torralva, B. R.; Allen, R. E. *J. Mol. Opt.* **2002**, *49*, 593. Dou, Y. S.; Torralva, B. R.; Allen, R. E. *J. Mod. Opt.* **2003**, *50*, 2615.

(9) Moad A. J.; Simpson G. J. *J. Phys. Chem. A* **2005**, *109*, 1316.

(10) Sugimori K.; Ito T.; Nagao H.; Nishikawa, K. *Int. J. Quantum Chem.* **2005**, *105*, 596.

(11) Gräfe S.; Erdmann M.; Engel V. *Phys. Rev. A* **2005**, *72*, 013404.

(12) Gibson G. N. *Phys. Rev. A* **2005**, *72*, 041404.

(13) Cabrera-Trujillo, R.; Ohrn, Y.; Deumens, E.; Sabin, J. R. *J. Phys. Chem. A* **2004**, *108*, 8935.

(14) Deumens, E.; Ohrn, Y. *J. Phys. Chem. A* **2001**, *105*, 2660.

(15) Ohrn, Y.; Deumens, E. *J. Phys. Chem. A* **1999**, *103*, 9545.

(16) Micha, D. A.; Thorndyke, B. *Adv. Q. Chem.* **2004**, *47*, 293.

(17) Micha, D. A.; Yi, Z. G. *Int. J. Q. Chem.* **2000**, *77*, 367.

(18) Chen, G. H.; Mukamel, S. *Chem. Phys. Lett.* **1996**, *258*, 589.

(19) Tsiper, E. V.; Chernyak, V.; Tretiak, S.; Mukamel, S. *Chem. Phys. Lett.* **1999**, *302*, 77.

(20) Frisch, M. J.; Trucks, G. W.; Schlegel, H. B.; Scuseria, G. E.; Robb, M. A.; Cheeseman, J. R.; Montgomery, J. A., Jr.; Vreven, T.; Kudin, K. N.; Burant, J. C.; Millam, J. M.; Iyengar, S. S.; Tomasi, J.; Barone, V.; Mennucci, B.; Cossi, M.; Scalmani, G.; Rega, N.; Petersson, G. A.; Nakatsuji, H.; Hada, M.; Ehara, M.; Toyota, K.; Fukuda, R.; Hasegawa, J.; Ishida, M.; Nakajima, T.; Honda, Y.; Kitao, O.; Nakai, H.; Klene, M.; Li, X.; Knox, J. E.; Hratchian, H. P.; Cross, J. B.; Bakken, V.; Adamo, C.; Jaramillo, J.; Gomperts, R.; Stratmann, R. E.; Yazyev, O.; Austin, A. J.; Cammi, R.; Pomelli, C.; Ochterski, J. W.; Ayala, P. Y.; Morokuma, K.; Voth, G. A.; Salvador, P.; Dannenberg, J. J.; Zakrzewski, V. G.; Dapprich, S.; Daniels, A. D.; Strain, M. C.; Farkas, O.; Malick, D. K.; Rabuck, A. D.; Raghavachari, K.; Foresman, J. B.; Ortiz, J. V.; Cui, Q.; Baboul, A. G.; Clifford, S.; Cioslowski, J.; Stefanov, B. B.; Liu, G.; Liashenko, A.; Piskorz, P.; Komaromi, I.; Martin, R. L.; Fox, D. J.; Keith, T.; Al-Laham, M. A.; Peng, C. Y.; Nanayakkara, A.; Challacombe, M.; Gill, P. M. W.; Johnson, B.; Chen, W.; Wong, M. W.; Gonzalez, C.; Pople, J. A. *Gaussian 03*, revision C.02; Gaussian, Inc.: Wallingford, CT, 2004.

(21) Browne J. C. *J. Phys. Chem.* **1964**, *41*, 3495.

(22) Niikura, H.; Legare, F.; Hasbani, R.; Bandrauk, A. D.; Ivanov, M. Y.; Villeneuve, D. M.; Corkum, P. B. *Nature* **2002**, *417*, 917.